7.0 LIQUEFACTION AND LATERAL SPREADING

7.1 Introduction

Liquefaction is the process of porewater pressure increase and concurrent loss of strength and stiffness resulting from rapid loading of loose to medium dense cohesionless soils. Earthquake-induced liquefaction and lateral spreading occurred extensively along the coastline around Port-au-Prince Bay and inland along several rivers and streams, and was responsible for the severe damage at the Port au Prince port. The damage to the port is discussed in Section 6.0 Port Facilities and Coastal Infrastructure, while this section focuses on all other locations of liquefaction.

7.2 General Observations

Prior to arrival in Haiti, GEER team members identified numerous potential liquefaction-induced failures near the coastline, as shown in Figure 7.1. Potential liquefaction-induced failures were identified up to 38 km from the epicenter and up to 26 km from the fault trace. These data plot well within the boundaries for most distal liquefaction sites proposed by Ambraseys (1988) using worldwide data (Figure 7.2). As discussed by Olson et al. (2005), this suggests that the natural coastal and alluvial soils near Port-au-Prince Bay are only moderately susceptible to liquefaction, although liquefiable Quaternary sediments were generally noted only within short distances from the coast. Additionally, without any strong motion recordings from this event, the level and duration of shaking is unknown. The slip inversions for the event (see Section 2.0 Seismological Aspects) indicate that most of the earthquake energy was released in 6 to 8 seconds, which is relatively short for a M 7 earthquake. This short duration of shaking would have limited the number of cycles of loading and minimized the zones that experienced liquefaction.

Generally, observed liquefaction-induced failures occurred either in fill soils placed to reclaim land for urban areas (e.g., Port-au-Prince port) or in Holocene-active delta fan lobes in coastal areas near the mouths of streams emptying into Port-au-Prince Bay. The most susceptible deposits and largest lateral spreads occurred within active Holocene delta fan lobes between Petite Goave and L-acul where well-defined deltas exist where local streams discharge from a mountain front near the coast. The short distance between the mountain front and coast has not allowed significant sorting and grain size reduction in the delta lobes, such that the sediments consist predominantly layers of coarse to fine, sand and silty sand. In these areas, the alluvial soils may have been deposited in a relatively loose state prior to being potentially densified by wave action. Further inland, liquefaction features were limited to the floodplains of lower-gradient, meandering streams occasionally found north and east of Port au Prince. Most of the streams along the southern rim of Port au Prince Bay are high-gradient, braided ephemeral streams that carry coarser sediment loads. Almost no liquefaction features were identified along these streams inland of the coastline. In the city of Port au Prince, most of the streams are rather shallow and ephemeral, and have been channelized and often lined with stones or concrete. As a result, liquefaction was unlikely to occur in these drainage channels. Furthermore, nearly all of the drainage channels became clogged with debris and trash following the earthquake. This precluded the team from identifying any potential liquefaction features using aerial photography or direct observation.

During the reconnaissance mission, the GEER team performed more detailed investigations of five potential liquefaction sites, namely the Port-au-Prince port, the coastal area north of the port, a coastal site near the village of L'acul, a coastal site near the village of Fouche, and a

coastal site near the village of Grand Goâve. The failures at the port and at the coastal area immediately north of the port are described in Section 6.0 of this report. The soils involved in these failures consisted of clean calcareous fill sands, likely placed by end-dumping. The remainder of this section focuses on the coastal failures involving natural sand deposits.

Figure 7.1. Potential liquefaction, lateral spreading, and coastal failure sites identified from post-earthquake aerial photography (sites identified as open hexagons). Imagery courtesy of Google Earth.

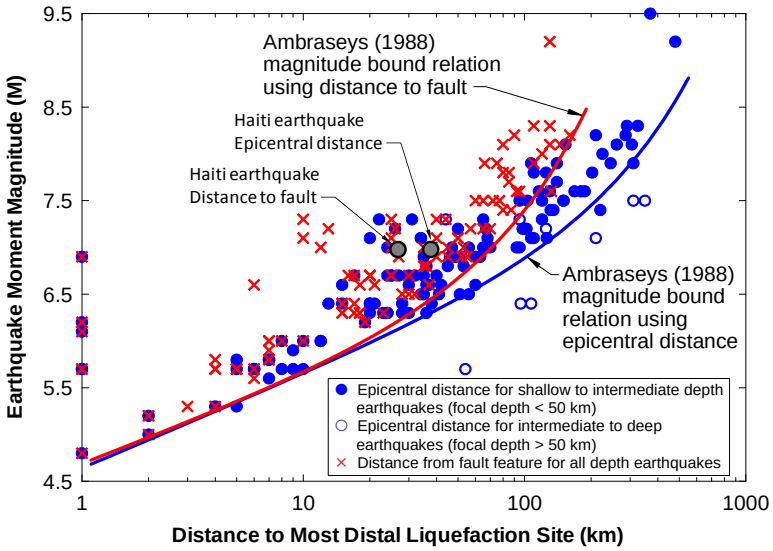

Figure 7.2. Comparison of most distal liquefaction sites identified in Haiti from aerial photography with worldwide data collected by Ambraseys (1988)

7.3 Coastal Failure west of L'acul

Approximately 400 m of coastline at the mouth of a stream experienced significant translational movement west of the village of L'acul, as illustrated by the pre- and post-earthquake imagery in Figure 7.3. Also evident near the south end of the failure are uplifted coral beds, as described Section 4.0 Fault Rupture and Coastal Uplift. The primary manifestations of failure included cracking subparallel to the coastline (Figure 7.4 and Figure 7.5), a slump block near the northern extent of the failed zone, and sand blows near the southern extent of the failed zone (Figure 7.6). It is important to note that lateral spreads typically occurred in delta fan lobes or beach deposits adjacent to major stream discharge/delta zones. Lateral spread failures were rare or absent at points where coral has developed and "buttressed" the shoreline.

During reconnaissance efforts, the team conducted two dynamic cone penetration tests (DCPT) and two spectral analysis of seismic waves (SASW) lines at the site, one set near the sand blows at the southern end of the failed zone and one set outside of the failed zone to the south (Figure 7.3). Figure 7.7 presents the results of the DCPTs. As illustrated in Figure 7.7, the stratigraphy changes dramatically between the failed and non-failed zones, with loose sands being encountered near-surface within the failed zone and clays and peats being encountered near-surface outside of the failed zone. The fine-grained stratigraphy is expected because of its significant distance from the active mouth of the stream to the north. The results from SASW testing are still being processed and will be included in future versions of this report.

Based on the subparallel cracking, the formation of sand blows, and the results of the in-situ tests, the team attributed this failure to liquefaction and lateral spreading. Liquefaction likely occurred within the loose to medium dense sands below the watertable between depths of about 0.75 m and 2.3 m (2.5 to 7.5 ft). Below 2.3 m in the failed zone, the DCPT encountered much denser sands. The extent of the failure to the south was limited by the presence of fine-grained soils and peat overlying the denser marine sands.

Figure 7.3. Pre- and post-earthquake images of coastline near village of L'Acul. Note in the lower, post-earthquake image the significant cracking subparallel to the coast and the arcuate slump in the northern end of the failure. SASW and DCPT testing was performed near several large sand blows located near the south end of the failure zone, as well as farther south outside of the failed reach. Imagery courtesy of Google Earth. Approximate center of image at 18°26'51.17"N, 72°41'11.06"W.

Figure 7.4. Cracking and lateral spread along coastline near village of L'Acul. (18°26'48.81"N, 72°41'11.92"W looking west).

Figure 7.5. Ground cracking along coastline near village of L'Acul. (18°26'48.83"N, 72°41'11.39"W looking west).

Figure 7.6. Sand blow formation to the south of the main cracks along coast near village of L'Acul. (18°26'44.27"N, 72°41'12.05"W looking south).

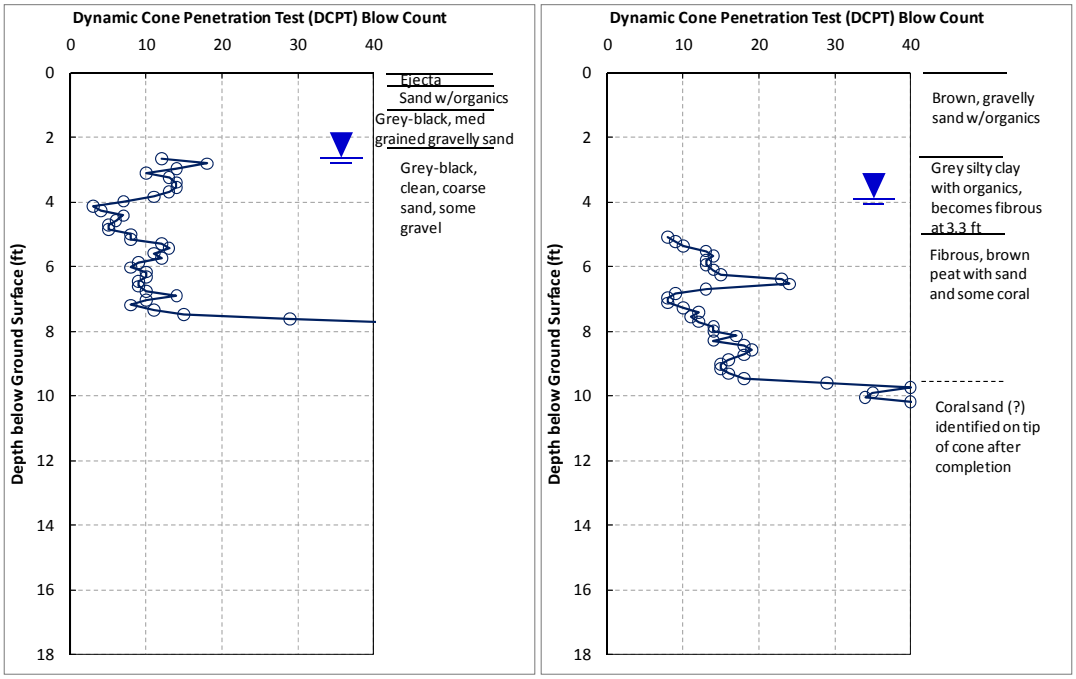

Figure 7.7. Results of DCPTs performed near coastline near village of L'Acul. Sounding on left performed at south end of failed zone (DCPT-8), and sounding on right performed outside of failed zone (DCPT-9).

7.4 Coastal Failure near Fouche

Approximately 330 m of coastline failed near the village of Fouche, as illustrated in pre- and post-earthquake imagery in Figure 7.8. At this site, as much as 100 m of land (perpendicular to the coast) was lost as a result of the failure. The primary manifestations of failure included scarps, cracking, and graben formation in an arcuate path along the coastline (Figure 7.9 and Figure 7.10), as well as substantial damage to a stone wall running perpendicular to the coast and parallel to a braided stream that emptied into the bay (Figure 7.11 and Figure 7.12) and moderate-sized sand blows along the inland extent of the failure (Figure 7.13). One sand blow area included gravel clasts of up to about 2.5 cm in maximum dimension. The gravels may have been plucked from the sidewalls of the liquefaction feeder dike/fissure, or could have been entrained in the actual liquefied sediments.

During the reconnaissance efforts, the team conducted one DCPT and one SASW line near several sand blows at the eastern end of the failed zone (Figure 7.8 and Figure 7.14), and one SASW line outside of the failed zone to the east (Figure 7.8). A second DCPT was attempted in this non-failed area but a thick layer of fill precluded augering beyond a few inches. Figure 7.15 presents the results of the DCPT in the failed zone. As illustrated in Figure 7.15, loose sand was encountered at a depth of about 0.7 m (2.5 ft), underlying a low permeability cap layer consisting of clayey sand and silty clay. The sands became medium-dense to dense at a depth of about 1.6 m (5.5 ft). The results from SASW testing are still being processed and will be included in future versions of this report.

Based on the arcuate scarp, graben formation, sand blows development, and the results of the in-situ tests, the team attributed this failure to liquefaction and lateral spreading of the loose to medium dense sands below a depth of 0.7 m (2.5 ft). Headscarps and slump block scarps were up to 1.5 m high in the central parts of the failure, suggesting that failure extends perhaps 1.5 to 2 m below the original ground surface. Liquefaction likely extended to a depth of 1.6 m and may have occurred at greater depth, but penetration with the DCPT was limited in these denser sands. Similar to the coastal failure near the village of L'acul, this failure appears to coincide directly with the presence of the braided stream dumping loose sand into the sea, rather than in the marine sands present along the coast.

Figure 7.8. Pre- and post-earthquake images of coastline near village of Fouche. Note in the lower, post-earthquake image the significant loss of coast as outlined in blue. SASW-9 and DCPT-6 were performed near several moderate-sized sand blows located near the southeast end of the failure zone, while SASW-10 was performed outside of the failure zone. Imagery courtesy of Google Earth.

Figure 7.9. Scarp of coastal landslide near village of Fouche.
(18°25'34.23"N, 72°43'33.61"W looking northeastward)

Figure 7.10. Scarp of coastal landslide near village of Fouche.
(18°25'34.01"N, 72°43'34.60"W looking westward).

Figure 7.11. Damage to stone wall resulting from coastal failure and lateral spreading. (18°25'33.94"N, 72°43'34.27"W looking westward).

Figure 7.12. Damage to stone wall resulting from lateral spreading. Note the surficial cobbly material revealed by the failure scarp in the foreground. (18°25'33.31"N, 72°43'34.58"W looking southward away from coast).

Figure 7.13. Sand blow and ejecta formed at coastal failure site near village of Fouche. Approximate image coordinates: 18°25'35.08"N, 72°43'31.70"W.

Figure 7.14. DCPT and SASW testing performed at coastal failure site near village of Fouche. Approximate image coordinates: 18°25'35.12"N, 72°43'31.61"W.

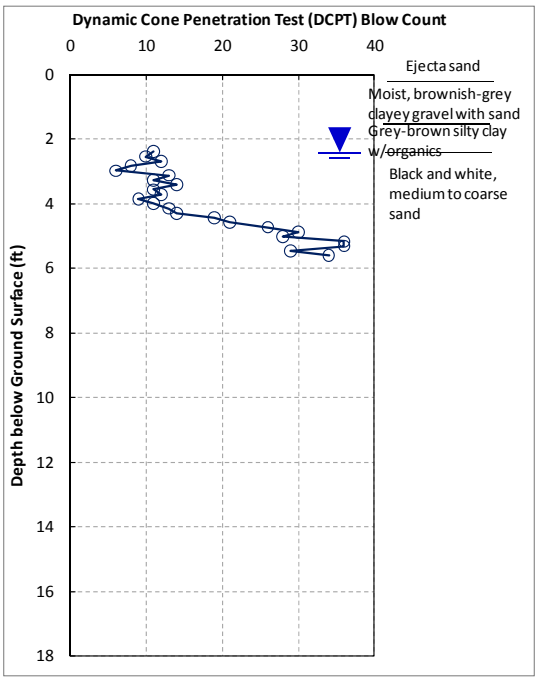

Figure 7.15. Results of DCPT-5 testing at coastal failure site near village of Fouche.

7.5 Coastal failure near Grand Goâve.

Approximately 400 m of coastline failed near the village of Grand Goâve, as illustrated in pre- and post-earthquake imagery in Figure 7.16. At this site, nearly 100 m of land (perpendicular to the coast) was lost as a result of the slide. The primary manifestations of failure included scarps (Figure 7.17 and Figure 7.18), cracking, and graben formation subparallel to the coastline (Figure 7.19), substantial damage to a unreinforced block wall running perpendicular to the coast (Figure 7.20), and small- to moderate-sized sand blows along the inland extent of the failure (Figure 7.21).

During reconnaissance, the team performed two DCPT and one SASW line near several sand blows at the inward end of the failed zone (Figure 7.16 and Figure 7.22). Figure 7.23 presents the results of the DCPT. As illustrated in Figure 7.23, loose sand to silty sand was encountered at a depth of about 0.8 to 0.9 m (2.6 to 3.0 ft), underlying a low permeability cap layer consisting of clayey silt. The sands became medium-dense to dense at a depth of about 1.1 to 1.6 m (3.6 to 5.3 ft). The results from SASW testing are still being processed and will be included in future versions of this report.

Based on the arcuate scarp, graben formation, sand blows development, and the results of the in-situ tests, the team attributed this failure to liquefaction and lateral spreading of the loose to medium dense sands and silty sands below a depth of 0.9 m. Liquefaction likely extended to a depth of 1.6 m and may have occurred at greater depth, but penetration with the DCPT was limited in these denser sands. Similar to the coastal failures near the villages of L'acul and Fouche, this failure occurred adjacent to a braided stream dumping loose sand into the bay (probably in a former channel of the stream), rather than in the marine sands present along the coast.

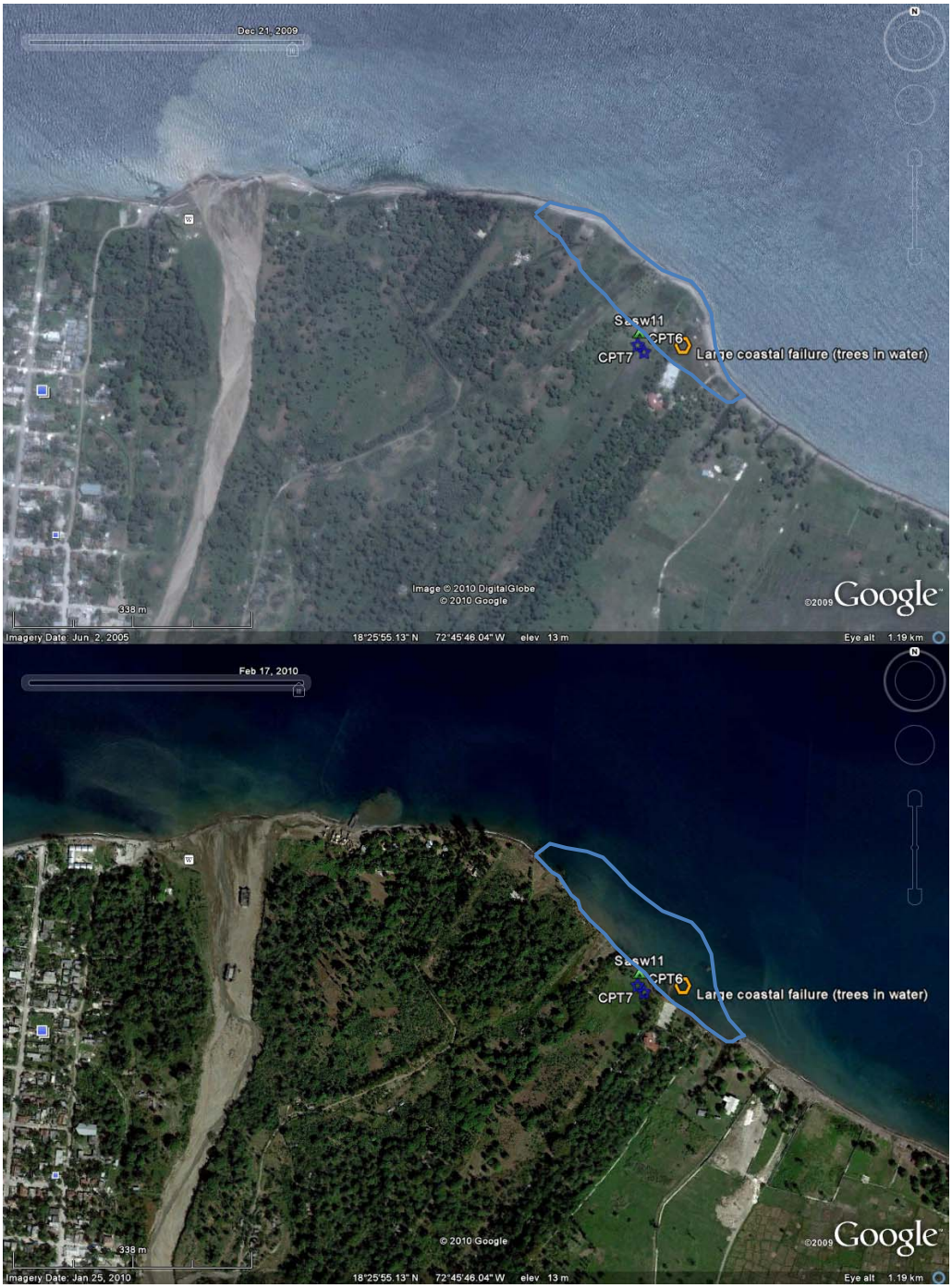

Figure 7.16. Pre- and post-earthquake images of coastline near village of Grand Goâve. Note in the lower, post-earthquake image the significant loss of coast as outlined in blue. SASW-11, DCPT-7, and DCPT-8 were performed just inland of the backscarp of the failed zone. Imagery courtesy of Google Earth.

Figure 7.17. Scarp formed along northern portion of coastal failure near village of Grand Goâve. (18°25'53.82"N, 72°45'37.16"W looking northwest).

Figure 7.18. Scarp formed along southern portion of coastal failure near village of Grand Goâve. (18°25'52.91"N, 72°45'35.92"W looking northwest)

Figure 7.19. Graben formation subparallel to coastline at coastal failure near village of Grand Goâve. (18°25'54.43"N, 72°45'37.99"W looking northwest).

Figure 7.20. Damage to unreinforced block wall running perpendicular to coast near village of Grand Goâve. (18°25'51.84"N, 72°45'38.06"W looking northeast).

Figure 7.21. Sand blow formation along inland extent of coastal failure near village of Grand Goâve. (18°25'53.73"N, 72°45'37.65"W)

Figure 7.22. DCPT and SASW testing at coastal failure site near village of Grand Goâve. (18°25'53.64"N, 72°45'37.76"W for left image, 18°25'54.16"N, 72°45'37.85"W for right image)

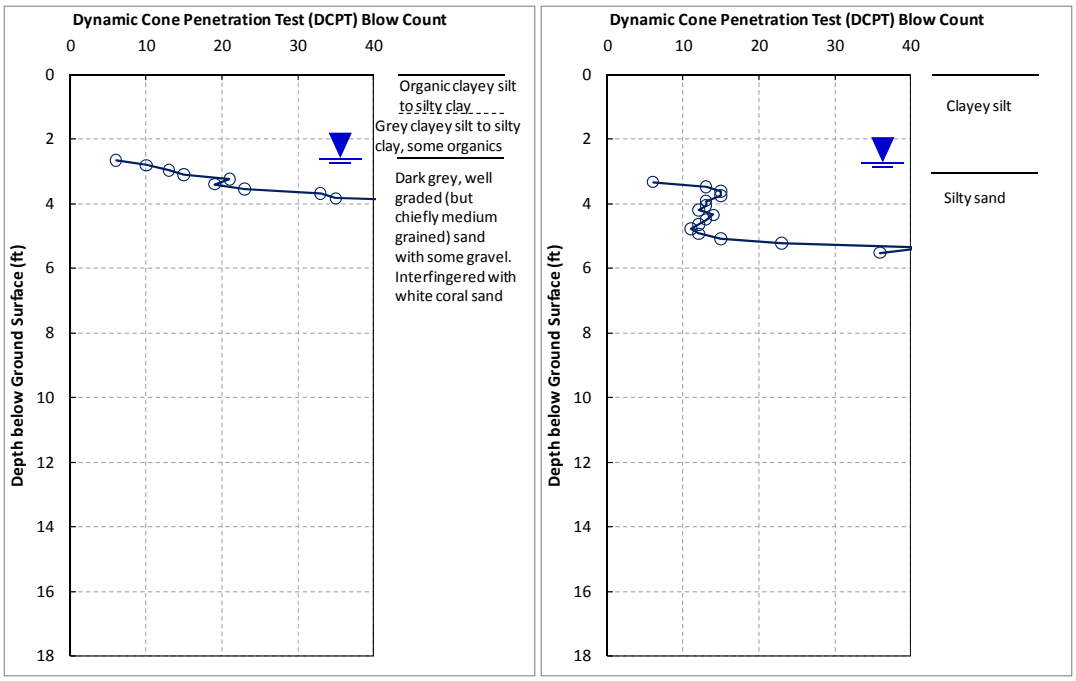

Figure 7.23. Results of DCPT-6 (at left) and DCPT-7 (at right) performed at coastal failure near village of Grand Goâve.

References

Ambraseys, N.N. (1988). Engineering seismology. Earthquake Engineering and Structural Dynamics, 17, 1-105.

Olson, S.M., Green, R.A., Obermeier, S.F. (2005). Revised magnitude-bound relation for the Wabash Valley seismic zone of the central United States. Seismological Research Letters, 76(6), 756-771.